crystals

MDPI

Article

Effects of Continuous Rolling and Reversible Rolling on 2.4% Si Non-Oriented Silicon Steel

Kaixuan Shao [1,2], Yuhao Niu [1,2,3], Yinghao Pei [4], Jialong Qiao [1,2,3,*], Hongbo Pan [1,2] and Haijun Wang [1,2]

[1] Anhui Key Laboratory of Low Carbon Metallurgy and Solid Waste Resource Utilization, Anhui University of Technology, Ma'anshan 243032, China; shao25802021@163.com (K.S.); niuyuhaoahut@163.com (Y.N.); 20130007@ahut.edu.cn (H.P.); whjchina@ahut.edu.cn (H.W.)
[2] School of Metallurgical Engineering, Anhui University of Technology, Ma'anshan 243032, China
[3] Iron and Steel Research Institute Co., Ltd., Beijing 100081, China
[4] Technology Center, Ma'anshan Iron and Steel Co., Ltd., Ma'anshan 243000, China; m76349@baosteel.com
* Correspondence: qiaojialong2015@126.com

Abstract: The cold-rolled non-oriented silicon steel sheets with a Si content of 2.4 wt.%, produced by continuous and reversible cold rolling, were used as the experimental material. The effects of annealing temperature on the microstructure, texture, and magnetic properties were studied by optical microscopy, an X-ray diffractometer, and a magnetic property measuring instrument. The experimental results showed that the dominant texture components at the surface of both sheets were almost the same, i.e., α and γ fibers. After annealing at 920 °C for 30 s, a complete recrystallization occurred in both sheets. When annealing below 1070 °C, the average grain sizes of continuous cold-rolled sheets were slightly higher than those of reversible cold-rolled ones. Additionally, for all specimens, the recrystallization texture components were γ fiber, as well as weak α fiber, λ fiber, and Goss texture. Additionally, the difference was the texture intensity. The iron losses of the finished products of continuous cold rolling were lower than those of the finished products of reversible cold rolling with the increase in annealing temperature, and the magnetic induction was higher than that of the finished products of reversible cold rolling.

Keywords: non-oriented silicon steel; iron loss; magnetic induction; cold rolling; texture

check for updates

Citation: Shao, K.; Niu, Y.; Pei, Y.; Qiao, J.; Pan, H.; Wang, H. Effects of Continuous Rolling and Reversible Rolling on 2.4% Si Non-Oriented Silicon Steel. *Crystals* **2024**, *14*, 824. https://doi.org/10.3390/cryst14090824

Academic Editor: José L. García

Received: 21 August 2024
Revised: 10 September 2024
Accepted: 13 September 2024
Published: 20 September 2024

Copyright: © 2024 by the authors. Licensee MDPI, Basel, Switzerland. This article is an open access article distributed under the terms and conditions of the Creative Commons Attribution (CC BY) license (https://creativecommons.org/licenses/by/4.0/).

1. Introduction

Cold-rolled non-oriented silicon steel is a kind of Fe-Si-Al alloy with an extremely low carbon content and a total mass fraction of Si and Al ranging from approximately 1.5 to 4.0%. It is widely used as the core of medium and large motors and generators because of its ability to maintain excellent magnetic isotropy in all directions in a high-speed rotating magnetic field. In addition, it offers a higher performance price ratio compared with iron-based amorphous alloys, dual-phase materials, nanocrystalline alloys, and other core magnetic materials [1–3]. In recent years, the drive motors of new energy vehicles require non-oriented silicon steel to meet the magnetic properties of high magnetic induction, low iron loss, and low magnetostriction. At the same time, non-oriented silicon steel needs to have high mechanical properties, such as yield strength and tensile strength, to resist the deformation and fatigue fracture caused by the centrifugal force when the motor is running at a high speed [4–6].

For non-oriented silicon steel, it is typically desired to maximize {100} planes during the cold rolling and annealing process, while minimizing {111} planes as much as possible [7]. Kawamata et al. [8] used rolls with three different radii to carry out cold rolling experiments on hot-rolled sheets with two different thicknesses. The results showed that when the roller shape parameter was smaller, the development of surface γ fiber (<111>//ND) after annealing of the cold-rolled sample was suppressed, while the vicinity 0of the {100} <001> component was developed. Cheong et al. [9] studied the effects of roll roughness on texture

and magnetic properties. Compared with the rough work roll, the smooth work roll made the surface stress of the rolled piece more concentrated, resulting in sharper textures of the rolled piece. When Li et al. [10] annealed 2.8 wt.% Si non-oriented silicon steel at 1100 °C, the Goss ({110} <001>) and Cube textures ({001} <100>) were stronger and {111} <112> was weaker in the grain growth stage. With the increase in annealing time, the intensity of the Cube texture increased with the grain growth, the intensity of Goss texture decreased obviously, and the intensity of {111} <112> did not change significantly. Kestens et al. [11] used "cross rolling" to rotate the hot-rolled sheet around ND (normal direction) by 90° before cold rolling, switching RD (rolling direction) and TD (transverse direction), and finally formed a very strong Cube texture or Rotated Cube texture ({001} <110>) in the sheet.

At present, the large-scale production of cold-rolled non-oriented silicon steel mainly adopts continuous cold rolling. However, due to the reasons of manufacturing cost, work efficiency, and market demand, the non-oriented silicon steel products produced by reversible cold rolling have the characteristics of a small batch, multi-variety, and short cycle, so they also occupy a place in the user market. Most of the existing research focuses on the effect of the annealing process on the grain size, texture strength, and magnetic properties of non-oriented silicon steel under a certain cold rolling method. In addition, different grades of non-oriented silicon steel have different cold rolling reduction rates in the production process. The change in the cold rolling reduction rate will directly affect the deformation microstructure, thus affecting the formation of recrystallized grains and then changing the magnetic properties. Therefore, it is of great significance to study the effects of different cold rolling methods and cold rolling reduction rates on the deformation structure and texture, recrystallization texture evolution, and magnetic properties of non-oriented silicon steel cold-rolled sheets.

In this work, the same furnace non-oriented silicon steel produced by industrial production was selected and cold rolled to 0.35 mm by continuous and reversible cold rolling. After the same annealing process in the laboratory, the microstructure, texture, and magnetic properties of different annealed sheets were investigated. The aim is to clarify the changes of microstructure, texture, and magnetic properties of a 2.4% Si non-oriented silicon steel obtained by different cold rolling working systems after annealing.

2. Materials and Methods

The experimental material is the industrial production of the same furnace non-oriented silicon steel with a Si content of 2.4 wt.%, and the main chemical composition is shown in Table 1. The hot-rolled sheets of non-oriented silicon steel with a thickness of 2.20 mm were normalized at 900 °C for 3 min and then acid pickled in HCl aqueous solution with a volume fraction of about 10% at 60 °C for 10 min. At the end of pickling, the normalized sheets were rolled to 0.35 mm by continuous cold rolling and reversible cold rolling, respectively. The main frame of the reversible cold rolling mill mainly includes the upper and lower working rolls, sets the target reduction thickness in the mill control system, and starts the main mill to start the first pass rolling. When the strip is completely removed from the work roll, the main drive slows down and begins to reverse the next pass of rolling [12]. Then, the cold-rolled sheets were processed into Epstein square specimens with dimensions of 30 mm × 320 mm, and the annealing experiments were carried out in an RDM-180-11Q multi-atmosphere continuous annealing furnace. The specific annealing experimental processes are shown in Figure 1. The cold-rolled specimens were heated from room temperature to 800 °C at a heating rate of 20 °C·s^{-1} and held at that temperature for 180 s, then they were heated to the target process temperature for 30 s and slowly cooled to room temperature with the furnace. In addition, a dry mixed atmosphere of 20 vol.% H_2 + 80 vol.% N_2 was introduced throughout the furnace as a protective atmosphere for recrystallization annealing.

Table 1. Chemical composition of experimental raw materials (wt.%).

Elements	C	Si	Mn	P	S	Als	N	Ni	Cu	Ti	Nb
Content	0.0012	2.40	0.20	0.0008	0.0014	1.05	0.0011	0.0125	0.025	0.0023	0.0018

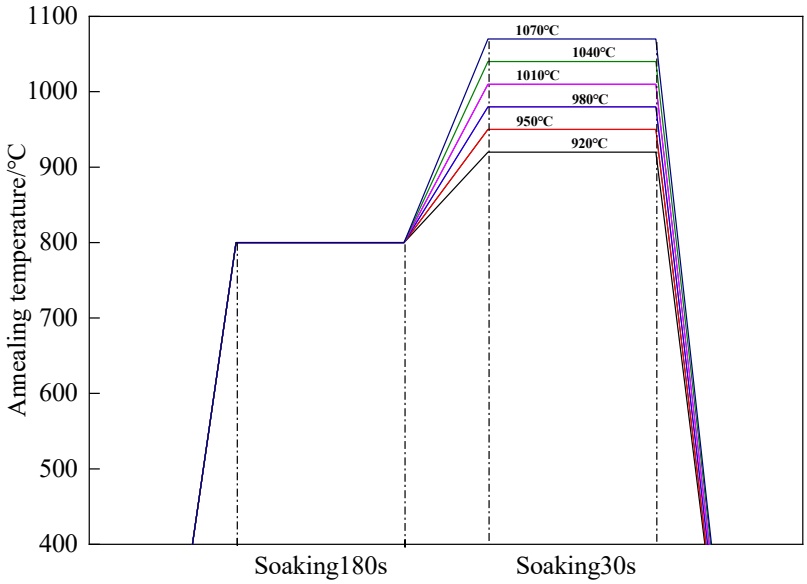


Figure 1. Laboratory annealing process diagram.

After annealing at different temperatures, the microstructures and textures of annealed sheets were observed, and the magnetic properties of the finished products were measured. The 15 mm (TD) × 20 mm (RD) specimens were used for microstructure observation. After standard grinding and polishing, the annealed samples were etched with a 5% nitric acid alcohol solution. The microstructures of the annealed sheets in the thickness direction were observed and captured on the ZEISS-200MAT metallographic microscopy (Tokyo, Japan) under 100× magnification. According to the cut-off point method in the GB/T6394-2002 metal average grain size measurement method, the image processing software Image Pro Plus 6.0 was used to measure the average grain size of the annealed specimens. Three to five fields of view were randomly selected for our statistics. In order to make the measurement results more accurate, the number of cut-off points for each specimen should reach 500. The X' Pert Pro X-ray diffractometer was used to detect the macro-textures at the surface layer of different annealed sheets of 15 mm (TD) × 20 mm (RD). The X-ray diffractometer uses a CoKα radiation source with a tube voltage of 35 kV and a tube current of 40 mA. The orientation distribution functions (ODFs) were calculated from {200}, {110}, and {211} incomplete pole-figures, and the orientation distribution function was calculated by X' Pert Texture software.

The magnetic properties were measured by the Epstein square method. Eight pieces of 30 mm (TD) × 320 mm (RD) specimens were measured on the Metron SKJ-300 magnetic performance measuring instrument (Tokyo, Japan) according to GB/T3655. The magnetic properties of the finished products after annealing at different temperatures were measured. Specifically, the iron loss at 1.5 T by 50 Hz ($P_{1.5/50}$) and magnetic induction at 5000 A·m^{-1} (B_{50}) were measured, respectively.

3. Experimental Results

3.1. Textures of Hot-Rolled and Normalized Sheets

The ODFs for the $\Phi_2 = 45°$ section at the surface layer of hot-rolled and normalized sheets of 2.36% Si non-oriented silicon steel are shown in Figure 2, and the observation surface is RD-ND. The surface texture of the hot-rolled sheet is dominated by a strong Goss

texture, and it contains a weak α texture and λ texture. Due to the contact between the surface layer and the roll, the friction generates strong shear stress to form a typical Goss texture [13]. Figure 2b shows that the surface texture of the normalized sheet is similar to that of the hot-rolled sheet. The normalized sheet is mainly composed of {110} <112>~{110} <001> and {111} <110>~{111} <112>. The orientation density of the Goss texture decreases from 3.4 in the hot-rolled sheet to 3.0, but the distribution of the {111} <112> and {111} <110> textures is more concentrated than that of the hot-rolled sheet, and the texture orientation density reaches 2.1 and 1.2, respectively.

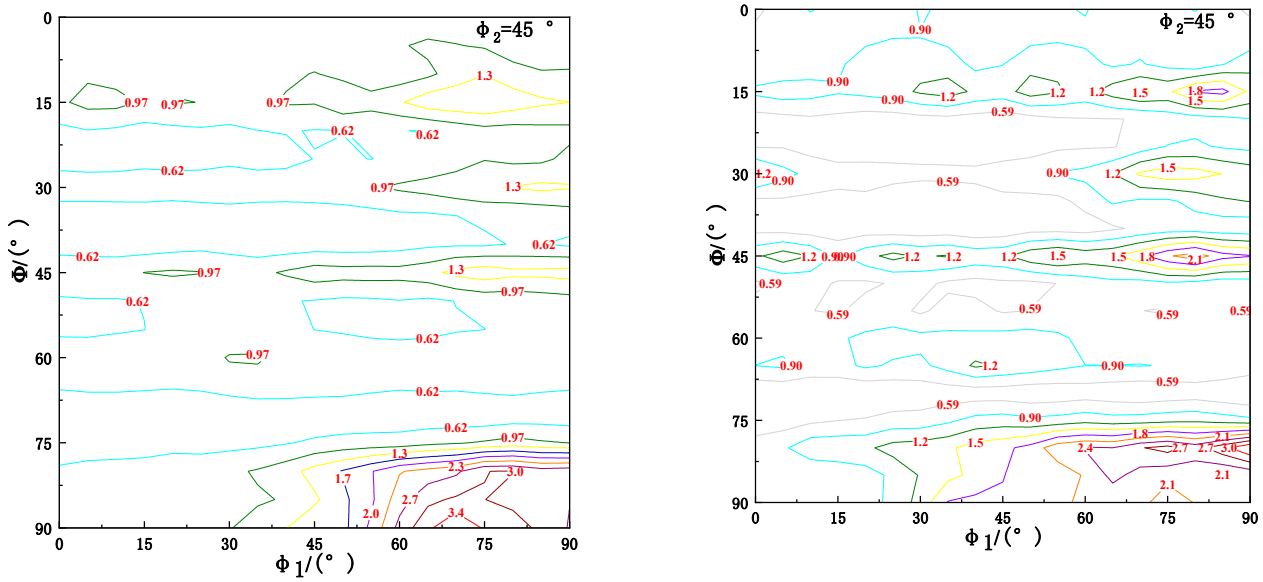


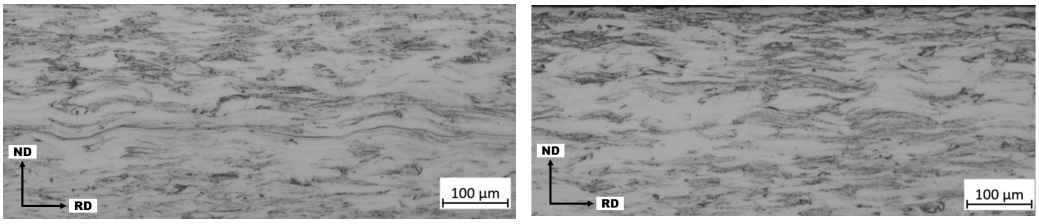
Figure 2. Textures in the surface layer of hot-rolled and normalized sheets. (**a**) Hot-rolled sheet and (**b**) normalized sheet. The numbers in the figures are texture intensities.

3.2. Microstructures and Textures of Cold-Rolled Sheets

Figure 3 shows the optical microscopy (OM) images of the continuous cold-rolled sheet and reversible cold-rolled sheet, and the observation surface is RD-ND. The microstructures of hot-rolled sheets after normalization are generally recrystallized ferrite. Due to the effect of the external load during cold rolling, the ferrite grains have undergone different degrees of deformation. The compression deformation is a fibrous mixed structure, and the grain boundaries are difficult to distinguish. According to the report of Hu et al. [14], strong α fiber (<110>//RD) and weak γ fiber were formed after the cold rolling of a normalized sheet. Due to the different chemical reaction rates of grains with different orientations during the corrosion process, the corrosion of {111} grains are the fastest. In order to preliminarily judge the intensity of each texture after cold rolling, the metallographic structure of cold-rolled sheets is observed after erosion with 4 vol.% nitric acid + 96 vol.% alcohol. In Figure 3a,b, the area with lighter color is larger, and the area with darker color is less. Therefore, it is preliminarily judged from the degree of corrosion that the γ fiber of the two cold-rolled sheets is weak, and shear bands are usually formed in the deformed γ-fiber grains, which are fishtailed in the deformed structure.

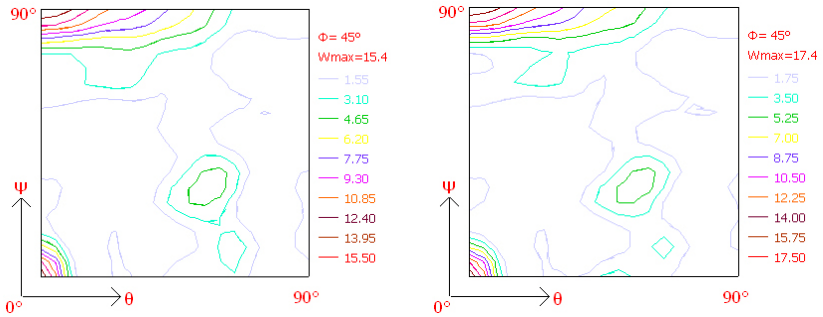
Figure 4a,b show the ODFs for the Φ = 45° section at the surface layer of normalized sheets after continuous cold rolling and reversible cold rolling, respectively. Whether it is continuous cold rolling or reversible cold rolling, the dominant components after cold rolling accumulate on the α-fiber and γ-fiber orientations, which have a typical body-centered cubic metal rolling texture. The {001} <110>, {113} <110>, and {111} <110> orientations are relatively concentrated [15]. The α-fiber intensity in cold-rolled textures is stronger than the γ-fiber intensity. The texture intensities formed by reversible cold rolling

in α fiber are stronger than those formed by continuous cold rolling, such as {001} <110> and {112} <110>, indicating that reverse cold rolling is more favorable for the formation of the α fiber. The texture types of the cold-rolled sheets by continuous and reversible cold rolling are basically the same, and both have a strong Rotated Cube texture ({001} <110>).



(**a**) (**b**)

Figure 3. Microstructures of continuous cold-rolled sheet and reversible cold-rolled sheet. (**a**) Continuous cold-rolled sheet and (**b**) reversible cold-rolled sheet.



(**a**) (**b**)

Figure 4. Surface textures of continuous cold-rolled sheet and reversible cold-rolled sheet. (**a**) Continuous cold-rolled sheet and (**b**) reversible cold-rolled sheet.

3.3. Microstructures and Textures of Annealed Sheets

Figure 5 shows the microstructures of continuous cold-rolled sheets and reversible cold-rolled sheets after annealing. The grains of 2.4% Si non-oriented silicon steel annealed at 920 °C have completed recrystallization, resulting in a single ferrite structure, and some recrystallized grains have grown. After annealing at 1070 °C, the fine grains almost disappear and the microstructure uniformity is improved, but the grain size of the surface region is still slightly lower than that of the central layer [4]. Figure 6 shows the average grain size of the annealed sheets at different temperatures. The average grain sizes of the reversible cold-rolled sheets annealed at 920~950 °C are similar to those of the continuous cold-rolled annealed sheets. As the temperature gradually increases to 1010 °C, the difference of the average grain size between the two specimens at the same temperature increases. The average grain size of the reversible cold-rolled annealed sheet exceeds that of the continuous cold-rolled annealed sheet annealed at 1070 °C [16].

Table 2 shows the ODFs for the Φ = 45° section at the surface layer of continuous cold-rolled sheets and reversible cold-rolled sheets after annealing at different temperatures. The main recrystallization texture component is γ fiber with peak at {111} <112>, as well as a weak α fiber, λ fiber (<001>//ND), and Goss texture. For the annealed sheets of continuous cold rolling, with the increase in annealing temperature, the intensity of the {111} increases first and decreases, and reaches its maximum when annealed at 980 °C. The intensity of {001} <110> in the α fiber fluctuates with the increase in temperature, and it reaches maximum annealing at 980 °Cand reaches its maximum when annealed at 980 °C. The changes in the {110} and Goss textures are not obvious in the whole annealing temperature range. The intensities of the annealed sheets of reversible cold rolling are similar to those of the annealed sheets of continuous cold rolling, but the intensity of the {111} texture of the annealed sheets with reversible cold rolling reaches the maximum when

annealed at 950 °C, and the γ-fiber intensity of the two types of annealed sheets is not much different.

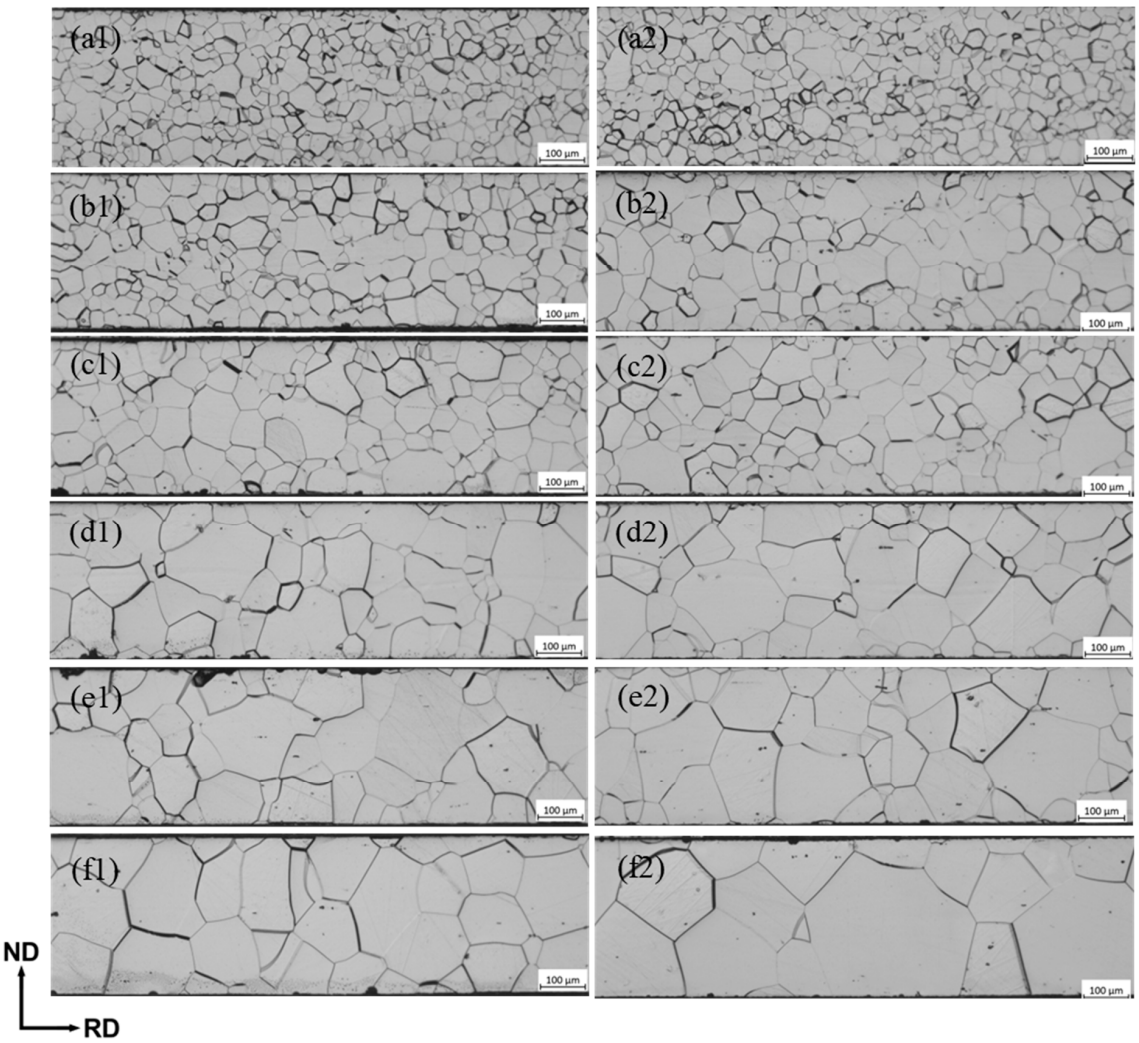


Figure 5. Microstructures of annealed sheets. (**a1**–**f1**) annealed sheets with continuous cold rolling; (**a2**–**f2**) annealed sheet with reversible cold rolling; (**a1**,**a2**) 920 °C; (**b1**,**b2**) 950 °C; (**c1**,**c2**) 980 °C; (**d1**,**d2**) 1010 °C; (**e1**,**e2**) 1040 °C; and (**f1**,**f2**) 1070 °C.

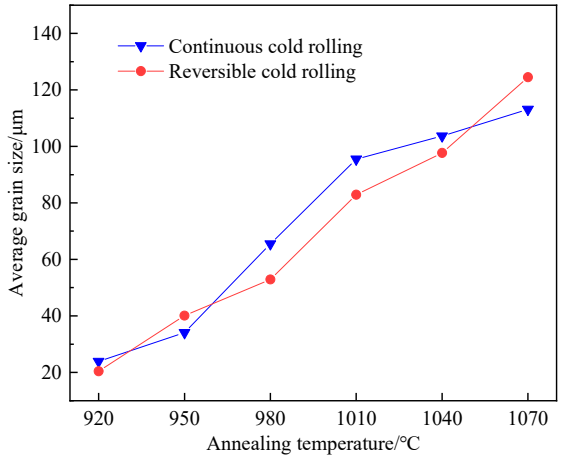


Figure 6. Average grain size of annealed sheets at different temperatures.

Table 2. Orientation distribution functions for a Φ = 45° section after annealing at different temperatures.

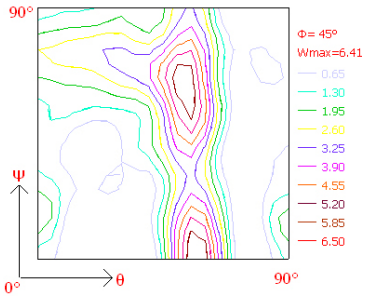
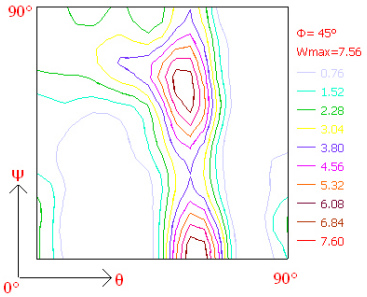
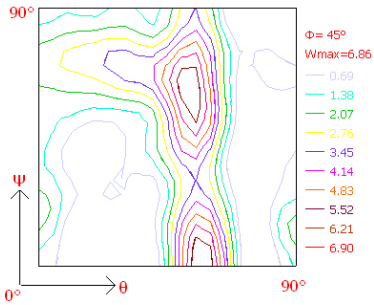
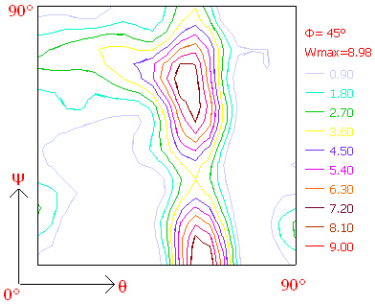
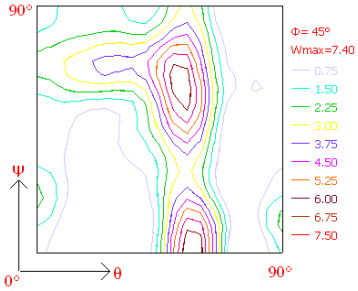
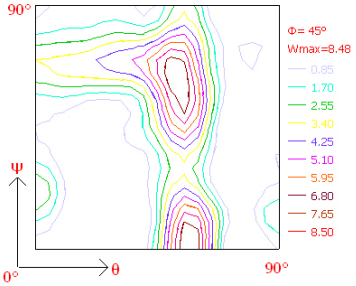
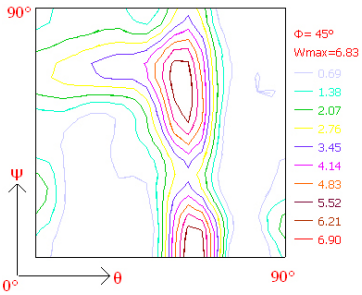
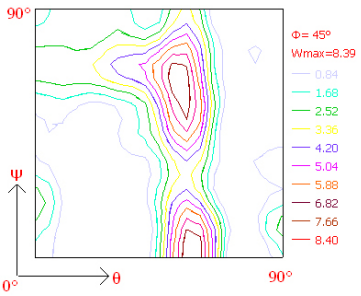
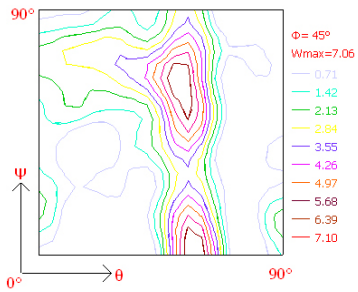
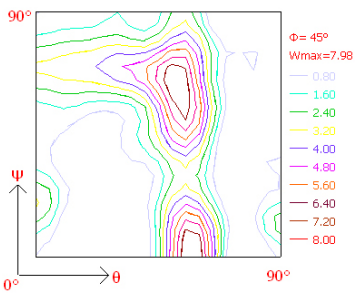
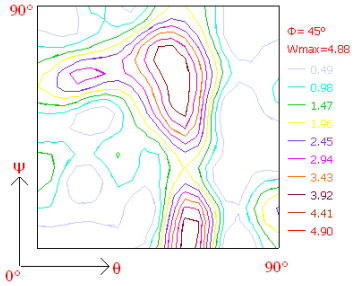
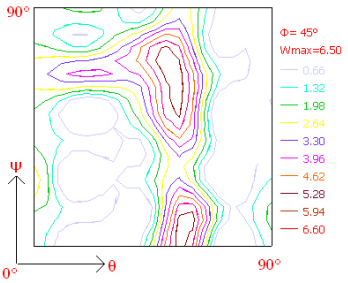
Temperature/°C	Cold Rolling Method	
	Continuous Cold Rolling	**Reversible Cold Rolling**
920		
950		
980		
1010		
1040		

Table 2. *Cont.*

Temperature/°C	Cold Rolling Method	
	Continuous Cold Rolling	Reversible Cold Rolling
1070		

3.4. Magnetic Properties of Annealed Finished Products

Figure 7 shows the magnetic induction and iron losses of the finished products. For the finished products of continuous cold rolling, with the increase in temperature, there is only a slight fluctuation in the overall magnetic induction B_{50}, with a small variation around 1.682 T, while the iron loss $P_{1.5/50}$ decreases. The specific performance is that the iron loss decreases sharply from 3.297 W·kg^{-1} to 2.922 W·kg^{-1} when annealed at 950 °C, and then it decreases slowly to the lowest value of 2.445 W·kg^{-1}. When the temperature rises to 1070 °C, the iron loss increases slightly to 2.494 W·kg^{-1}.

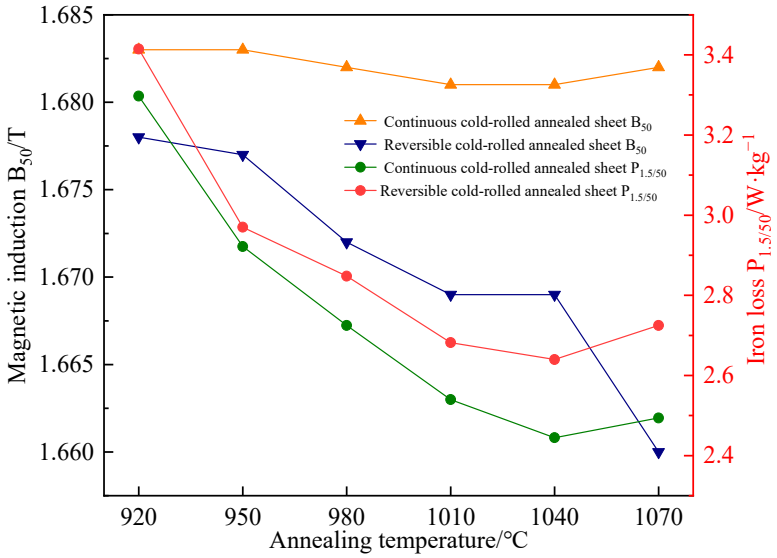


Figure 7. Iron losses $P_{1.5/50}$ and magnetic induction B_{50} of 2.4%Si non-oriented silicon steel after different annealing temperatures.

For the finished products of reversible cold rolling, the change trend of magnetic induction B_{50} is obviously different from that of continuous cold rolling. With the increase in annealing temperature, the magnetic induction B_{50} decreases slowly. When annealed at 1010 °C, the magnetic induction B_{50} decreases seriously and then tends to be stable at 1040 °C. However, when the temperature rises to 1070 °C, the magnetic induction B_{50} drops sharply to 1.660 T. The change trend of iron loss $P_{1.5/50}$ of the finished sheets of reversible cold rolling is similar to that of the finished sheets of continuous cold rolling, showing a trend of decreasing first and then increasing. The iron loss $P_{1.5/50}$ decreases slowly from 3.415 W·kg^{-1} to 2.640 W·kg^{-1}. When the annealing temperature rises to 1070 °C, the iron loss $P1_{.5/50}$ reaches 2.725 W·kg^{-1}.

Overall, the iron losses of the finished products of continuous cold rolling are lower than those of the finished products of reversible cold rolling with the increase in annealing temperature, and the magnetic induction is higher than that of the finished products of reversible cold rolling, because the crystallographic textures are important factors affecting the magnetic induction of non-oriented silicon steel, and the iron loss values are mainly determined by the grain sizes.

4. Analysis and Discussion

4.1. Effect of Cold Rolling Method on Microstructure and Texture

Plastic deformation occurs due to shear stress during the cold rolling of the normalized sheet, and the microstructure is mainly fibrous [17]. During polycrystalline rolling, deformation first occurs inside the grains. With the increase in rolling passes, the grains inside the sheet are elongated, and the dislocations are moved to the grain boundaries. The stress of the dislocations causes lattice distortion, and the internal strain-free subgrains are fibrous under the optical microscopy. The degree of tissue fibrosis is different between continuous cold-rolled sheet and reversible cold-rolled sheet due to different rolling methods. Figure 8 is a simplified diagram of the rolling deformation and stress of the polycrystalline sheet. Because the transverse direction of the sheet basically does not change, σ_{TD} is neglected. With the increase in rolling passes during continuous rolling, the influence of σ_{RD} on the deformation of the sheet during rolling is deepened, and additional shear stress is generated in the deformation zone to make each layer of metal slide along the rolling direction, so the effect of the shear stress is accumulated. In reversible rolling, the shear stress changes with the rolling direction, and the deformation effect of the shear force on the steel sheet during rolling cannot be accumulated. Therefore, under the same reduction rate, the degree of fibrosis of the transverse structure of the continuous cold-rolled sheet is less than that of the reversible cold-rolled sheet.

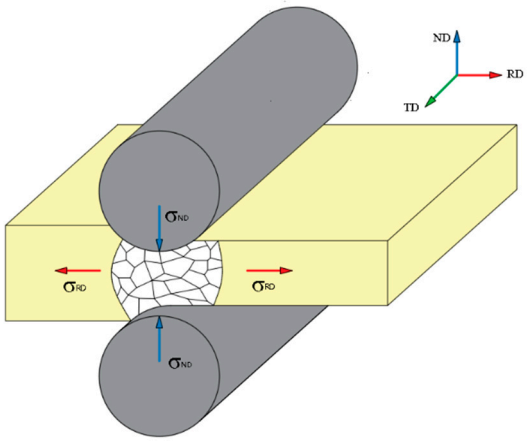


Figure 8. Simplified schematic diagram of rolling deformation and stress of polycrystalline sheet.

The shear stress effect of different rolling methods affects the grain rotation. The Bunge's symbol system was used to quantitatively analyze the texture intensity of each pass during the cross-section reduction process of the reversible cold-rolled sheet, and it is compared with the intensity of the 0.35 mm thick continuous cold-rolled sheet, as shown in Figure 9. After cold rolling with 65.91%, 70.45%, 80.91%, and 84.09% reduction, the normalized sheet formed strong α and γ fibers. The main textures in the α fiber are {001}~{112} <110>, and the main textures in the γ fiber are {111} <110> and {111} <112>. The reduction rate of the first pass of reversible cold rolling is 30.45%, the texture distribution is still relatively scattered, the grain orientation gradually gathers to the α-fiber orientation, the maximum value is near {001} <110>, and the γ-fiber intensity is weak. The second pass reduction rate is 65.91%. The strong intensity in the α fiber is near {112} <110>, and the maximum intensity in the γ fiber is near {111} <112>. The reduction rate of the third pass is

70.45%, and the grain orientations are completely concentrated near the α-fiber and γ-fiber orientations. The strong intensity at {112} <110> in the α fiber and the α fiber gradually moves to the {111} <110> orientation. The α-fiber and γ-fiber intensities increase at the same time. With the increase in the fourth pass reduction rate of 80.19% and the fifth pass reduction rate of 84.09%, the peak intensity of the reversible cold-rolled sheet appears near (0°, 15°, 45°), the intensity of {112} <110> decreases slightly, and the intensity of γ-fiber texture changes little. In the early stage of reversible cold rolling, the intensity of {001} <110> increases due to the shear stress, but the reversible cold rolling changes the direction of the surface shear stress. Therefore, with the increase in the rolling passes, the intensity of {001} <110> after rolling is weaker than that of the previous pass. The peak intensity of the α-fiber orientation of the continuous cold-rolled sheet is near {112} <110> and reaches 21. The peak intensity of the γ-fiber orientation is at {111} <110> and reaches 7.3. After the fifth pass rolling, the α-fiber intensity is significantly stronger than that of the reversible cold-rolled sheet, and the unfavorable {111} <112> is weaker than that of the reversible cold-rolled sheet [18,19].

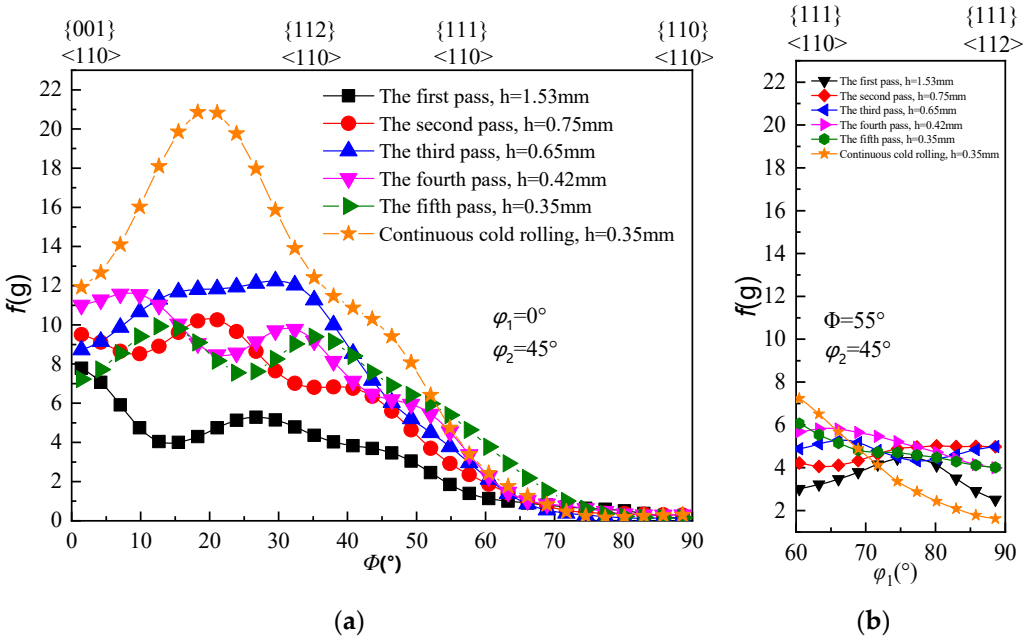


Figure 9. The density changes of α and γ fibers under different reduction rates. (**a**) The density changes of α fiber and (**b**) the density changes of γ fiber.

4.2. Effect of Annealing Temperature on Microstructure and Texture

The cold-rolled microstructures experienced recovery, recrystallization, and grain growth in the annealing stage. At the same annealing temperature, the average grain sizes of the annealed sheets are different, mainly due to the difference in rolling methods. The direction change of reversible cold rolling causes the grains to break into more shear bands, and the grains are more likely to nucleate at the shear bands during annealing. Reversible cold rolling has more nucleation points, resulting in the average grain sizes of the annealed sheets of continuous cold rolling being larger than those of the annealed sheets of reversible cold rolling [20]. However, with the increase in annealing temperature, the difference in average grain size between the two types of annealed sheets at the same temperature gradually decreases.

Figures 10 and 11 quantitatively show the variation of α-fiber and γ-fiber intensities of continuous cold-rolled sheets and reversible cold-rolled sheets with different annealing temperatures. The intensity of {00l} <110> increases first and then decreases with the increase in temperature during continuous cold rolling annealing, while it decreases rapidly and then increases slightly during reversible cold rolling annealing [21]. The main reason is that the deformation storage energy of grains is different. Due to the difference of the

microstructure and energy storage of deformed microstructure in cold-rolled sheets with different reduction rates, the order of deformation storage energy of grains with different orientations is [22] as follows: {001} < {112} < {111} < {110}.

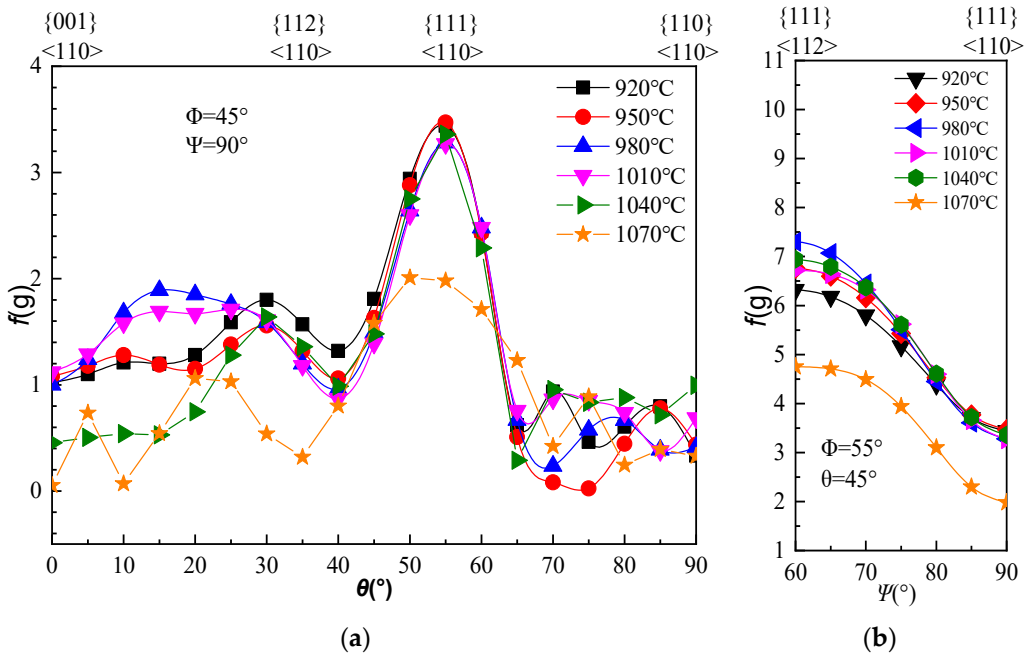


Figure 10. α and γ fibers of continuous cold-rolled sheets after different annealing temperatures. (**a**) α fiber of continuous cold-rolled sheets and (**b**) γ fiber of continuous cold-rolled sheets.

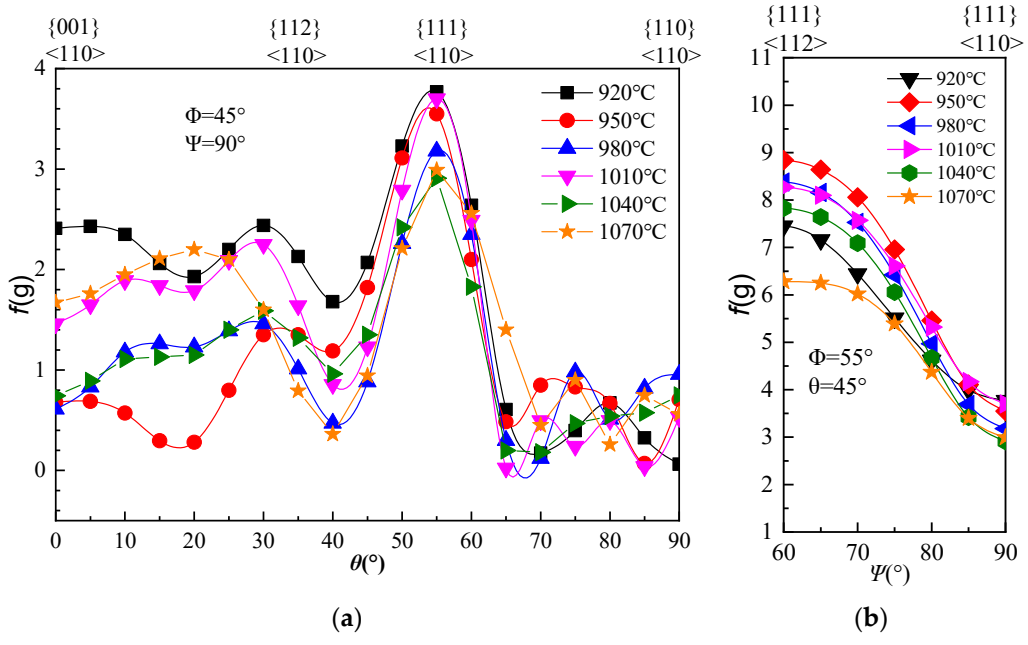


Figure 11. α and γ fibers of reversible cold-rolled sheets after different annealing temperatures. (**a**) α fiber of reversible cold-rolled sheets and (**b**) γ fiber of reversible cold-rolled sheets.

For a continuous cold-rolled sheet, after annealing at 920~1010 °C, {001} <110> grains are retained in situ recrystallization due to the low deformation storage energy, but the driving force of recrystallization is positively correlated with the annealing temperature. After annealing at 1040~1070 °C, the {001} <110> grains rotate to form other orientations, while the increase in the {001} <110> texture of the reversible cold-rolled sheet annealed at 1010 °C and 1070 °C is also due to the rotation of some grains to the {001} <110> orientation.

For both cold-rolled sheets, with the increase in annealing temperature, the α-fiber texture gradually gathers near the position of about 27° away from the <110> crystal axis due to the selective growth during recrystallization. [23]. It is not found in Figures 10 and 11 that the γ-fiber intensity increases monotonously with the increase in temperature. The main reason is that the storage energy along the γ-fiber orientation in the deformed matrix is high, and the {111} grains are recrystallized first, and the {111} texture is obviously enhanced due to the phagocytosis of the surrounding low storage energy grains. Similar results have been published for BCC Ti after cold rolling at 80% [24]. However, the preferential growth of {111} grains due to the high deformation storage energy is no longer obvious when the two cold-rolled sheets are annealed at 1070 °C and the γ-fiber intensity decreases [25].

4.3. Effect of Annealing Temperature on Magnetic Properties

{111} planes have the highest average magnetocrystalline anisotropy energy compared with {100} and {110} planes, which is one of the main factors affecting the magnetic induction [26,27]. For the non-oriented silicon steel with continuous cold rolling, combined with the findings in Figures 7 and 10, it can be seen that when the annealing temperature increases from 920 °C to 980 °C, the γ-fiber intensity increases gradually, and the α-fiber intensity remains basically unchanged, resulting in a decrease in B_{50}. When the annealing temperature rises to 1010 °C, the intensity of the {111} <110> texture remains basically unchanged, the intensity of the {111} <112> texture decreases slightly, and B_{50} increases. After annealing at 1070 °C, the γ-fiber intensity minimized more than that of the α fiber, and B_{50} increased slightly.

For reversible cold rolling (Figures 7 and 11), when the annealing temperature increases from 920 °C to 980 °C, the γ-fiber intensity increases first and then decreases, the α-fiber intensity decreases rapidly and then remains unchanged, and the intensity of {111} <110> decreases gradually, so B_{50} decreases. When the annealing temperature rises to 1070 °C, the γ-fiber intensity decreases significantly, the intensity of {111} <110> decreases and tends to be stable, and the α-fiber intensity increases slightly, but the magnetic induction B_{50} still decreases [28].

Hysteresis loss accounts for 55~75% of the power frequency iron loss $P_{1.5/50}$ of non-oriented silicon steel, which depends on the average grain size. In this work, the recrystallization of 2.4% Si non-oriented silicon steel was completed when annealed at 920 °C. With the increase in annealing temperature, the grain size increases, the area of the grain boundaries in the microstructure decreases, and the hysteresis loss decreases [29]. The grain size continues to increase, and the eddy current loss gradually increases, but the hysteresis loss still plays a leading role, and the total iron loss still decreases. When the grain size reaches the critical grain size, the magnetic domain size increases, resulting in the increase in eddy current loss and anomalous eddy current loss [30,31].

It can be seen from Figure 12 that the iron loss values of the two types of cold-rolled sheets after annealing decrease first and then increase with the increase in the average grain size. It is worth noting that for the annealed sheets of non-oriented silicon steel with two different cold rolling methods, when the average grain size is 82.9~113.1 μm, not only does the iron loss show a continuous downward trend, but it also has a high magnetic induction. When the average grain size is greater than 113.1 μm, the iron loss increases and the magnetic induction intensity decreases greatly, hence the overall magnetic properties deteriorate seriously. When the annealing temperature is between 1010 °C and 1040 °C, the iron loss $P_{1.5/50}$ tends to be stable. When the average grain size increases to a certain value, the iron loss $P_{1.5/50}$ increases. Comparing the iron losses $P_{1.5/50}$ of the two types of cold-rolled sheets after annealing, it is found that at the same annealing temperature, the average grain size of the annealed sheet of continuous cold rolling is higher than that of the annealed sheet of reversible cold rolling, so the iron loss of the annealed sheet of continuous cold rolling is slightly lower than that of the annealed sheet of reversible cold rolling, but the iron loss is not solely controlled by the size of grains. For example, after

annealing at 1070 °C, the average grain size of the annealed sheet of reversible cold rolling is higher, indicating that different rolling methods may affect the iron loss.

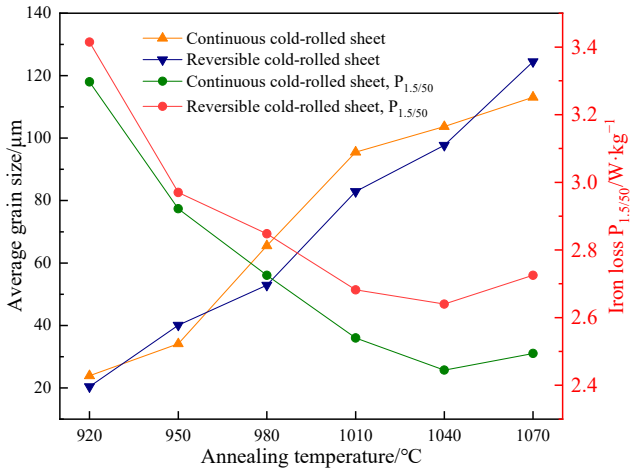


Figure 12. The average grain size and iron losses at different annealing temperatures.

5. Conclusions

(1) After the cold rolling of normalized sheets, the ferrite grains are deformed into flat or fibrous mixed structures. The surface textures of the two cold-rolled sheets are concentrated on the α-fiber and γ-fiber orientations, and the α-fiber intensity is significantly stronger than that of the γ fiber. The α-fiber intensity of the reversible cold-rolled sheet is stronger than that of the continuous cold-rolled sheet, and reversible cold rolling is more conducive to the formation of the α fiber.

(2) After annealing at 920 °C, the recrystallization process of the cold-rolled sheet is completed, and the average grain sizes increase with the increase in temperature. After annealing at different temperatures, the main recrystallization texture components are γ fiber, as well as a weak α fiber, λ fiber, and Goss texture.

(3) For two different cold-rolled non-oriented silicon steel annealed sheets, the critical grain size range should be 82.9~113.1 μm, and the overall magnetic performance is excellent. For the finished products of continuous cold rolling, the magnetic induction B_{50} fluctuates up and down at 1.682 T, and the iron loss $P_{1.5/50}$ drops to the lowest value of 2.445 W·kg^{-1}, which is annealed at 1040 °C. For the finished products of reversible cold rolling, the magnetic induction B_{50} is reduced to 1.660 T, annealed at 1070 °C, and the iron loss $P_{1.5/50}$ of the finished products is reduced to the lowest value of 2.640 W·kg^{-1}, which is annealed at 1040 °C.

(4) Under the condition of a certain chemical composition, with the increase in annealing temperature, the magnetic induction B_{50} of non-oriented silicon steel produced by reversible cold rolling is slightly lower than that of continuous cold rolling. If the product adopts continuous cold rolling, and is supplemented by a higher annealing temperature during annealing, lower amounts of iron loss can be obtained, and the comprehensive magnetic performance is the best. It is a method to improve the magnetic properties of products under the premise of certain chemical compositions. Therefore, in order to ensure the excellent electromagnetic properties of 2.36% Si non-oriented silicon steel, the continuous cold rolling method should be adopted, and the optimal annealing temperature should be controlled at 1010~1040 °C for 30 s.

Author Contributions: Conceptualization, K.S. and H.W.; methodology, Y.N and H.P.; software, J.Q.; validation, Y.N., Y.P. and H.W.; formal analysis, K.S.; investigation, K.S.; resources, Y.P.; data curation, Y.N., J.Q. and H.W.; writing—original draft preparation, K.S.; writing—review and editing, Y.N. and H.P.; visualization, H.W., Y.P. and H.P.; supervision, J.Q.; project administration, J.Q. and H.W.; and funding acquisition, H.W. All authors have read and agreed to the published version of the manuscript.

Funding: The authors acknowledge the support from the National Natural Science Foundation of China (No. 52374316), the Fund of Education Department of Anhui Province (No. 2022AH050291), the Open Project Program of Anhui Province Key Laboratory of Metallurgical Engineering & Resources Recycling (Anhui University of Technology) (No. SKF21-04 and SKF23-03), and the Jiangxi Province Major Scientific and Technological Research and Development Special Funding Project (20213AAE01009).

Data Availability Statement: The data presented in this study are available on request from the corresponding author due to privacy and ethical restrictions.

Conflicts of Interest: Authors Y.P. and J.Q. were employed by Ma'anshan Iron and Steel Co., Ltd. and Iron and Steel Research Institute Co., Ltd., respectively. The remaining authors declare that the research was conducted in the absence of any commercial or financial relationships that could be construed as potential conflicts of interest.

References

1. Zhu, C.Y.; Bao, Y.K.; Wang, Y.; Ma, J.H.; Li, G.Q. Research progress on application status and property control of non-oriented silicon steel for traction motor of new energy vehicles. *Mater. Rep.* **2021**, *35*, 23089–23096.
2. Zhu, C.Y.; Luo, X.Y.; Li, G.Q.; Feng, J.X.; Yan, Z.F. Formation mechanism analysis on magnesium-bearing inclusions in non-oriented silicon steels. *J. Chongqing Univ.* **2018**, *41*, 34–43.
3. Park, J.T.; Szpunar, J.A. Effect of initial grain size on texture evolution and magnetic properties in non-oriented electrical steels. *J. Magn. Magn. Mater.* **2009**, *321*, 1928–1932. [CrossRef]
4. Li, Z.H.; Xie, S.K.; Wang, G.D.; Liu, H.T. Dependence of recrystallization behavior and magnetic properties on grain size prior to cold rolling in high silicon non-oriented electrical steel. *J. Alloys Compd.* **2021**, *888*, 161576. [CrossRef]
5. Zhang, B.; Liang, Y.F.; Wen, S.B.; Wang, S.; Shi, X.J.; Ye, F.; Lin, J.P. High-strength low-iron-loss silicon steels fabricated by cold rolling. *J. Magn. Magn. Mater.* **2019**, *474*, 51–55. [CrossRef]
6. Fang, F.; Che, S.F.; Hou, D.W.; Zhang, Y.X.; Wang, Y.; Zhang, W.N.; Yuan, G.; Zhang, X.M.; Misra, R.D.K.; Wang, G.D. Thin-gauge non-oriented silicon steel with balanced magnetic and mechanical properties processed by strip casting. *Mater. Sci. Eng. A* **2022**, *831*, 142284. [CrossRef]
7. Li, M.; Xiao, Y.D.; Wang, W.; Zhou, J.; Wu, G.L.; Peng, Y.M. Effect of annealing parameter on microstructure and magnetic properties of cold-rolled non-oriented electrical steel. *Trans. Nonferrous Met. Soc. China* **2007**, *17*, s74–s78.
8. Kawamata, R.; Kubota, T.; Yamada, K. The effect of cold rolling parameters on the recrystallization texture of non-oriented electrical steel. *J. Mater. Eng. Perform.* **1997**, *6*, 701–709. [CrossRef]
9. Cheong, S.W.; Hilinski, E.J.; Rollett, A.D. Effect of temper rolling on texture formation in a low loss cold-rolled magnetic lamination steel. *Metall. Mater. Trans. A* **2003**, *34*, 1311–1319. [CrossRef]
10. Li, N.; Ma, L.; Xiang, L.; Qiu, S.T.; Zhao, P. Evolution of texture in a 2.8%Si non-oriented electrical steel annealed at 1100 °C. *Mater. Trans.* **2014**, *55*, 387–390. [CrossRef]
11. Kestens, L.; Jacobs, S. Texture control during the manufacturing of non-oriented electrical steels. *Texture Stress Micro.* **2008**, *2008*, 173083.
12. Zhang, S.R. Research on Rolling Force Prediction Method of Six-high Reversible Cold Rolling Mill. Master's Thesis, Xi'an University of Technology, Xi'an, China, 2021.
13. An, L.Z.; Wang, Y.P.; Song, H.Y.; Wang, G.D.; Liu, H.T. Improving magnetic properties of non-oriented electrical steels by controlling grain size prior to cold rolling. *J. Magn. Magn. Mater.* **2019**, *491*, 165636. [CrossRef]
14. Hu, C.Y.; Song, R.B.; Wang, Y.J.; Zhao, Z.Y.; Zhang, Y.C. Comprehensive influence of the normalized and final annealing process on high-strength non-oriented silicon steel. *Steel Res. Int.* **2022**, *93*, 2100641. [CrossRef]
15. Xin, Y.H.; Gao, Z.Y.; Huang, Y.Z.; Xu, H.J.; Xu, Y.B. Effect of annealing temperature on microstructure, texture and magnetic properties of non-oriented 3.2%Si steel. *Trans. Mate. Heat Treat.* **2021**, *42*, 74–80.
16. Schulte, M.; Steentjes, S.; Leuning, N.; Bleck, W.; Hameyer, K. Effect of manganese in high silicon alloyed non-oriented electrical steel sheets. *J. Magn. Magn. Mater.* **2019**, *477*, 372–381. [CrossRef]
17. Sanjari, M.; He, Y.L.; Hilinski, E.J.; Yue, S.; Kestens, L.A.I. Development of the {113}<uvw> texture during the annealing of a skew cold-rolled non-oriented electrical steel. *Scripta Mater.* **2016**, *124*, 179–183.
18. Peng, K.; Xiang, L.; Qiu, S.T.; Zhang, Y.H. Microstructure and texture of 50W470 silicon steel during reversing cold rolling process. *Heat Treat. Metals.* **2016**, *41*, 46–49.
19. Chu, S.J.; Shen, K.Y.; Sha, Y.H.; Chen, X. Orientation dependence of strain stored energy and its effect on recrystallization texture in non-oriented silicon steel. *J. Mater. Eng.* **2019**, *47*, 147–153.
20. Gupta, A.; Khatirkar, R.K.; Kumar, A.; Thool, K.; Bibhanshu, N.; Suwas, S. Microstructure and texture development in Ti-15V-3Cr-3Sn-3Al alloy–Possible role of strain path. *Mater. Charact.* **2019**, *156*, 109884. [CrossRef]
21. He, Z.Z.; Zhao, Y.; Luo, H.W. *Electrical Steel*; Metallurgical Industry Press: Beijing, China, 2012.
22. Park, J.T.; Szpunar, J.A. Evolution of recrystallization texture in non-oriented electrical steels. *Acta Mater.* **2003**, *51*, 3037–3051. [CrossRef]

23. Kestens, L.; Jonas, J.J. Modelling texture change during the static recrystallization of a cold-rolled and annealed ultra low carbon steel previously warm rolled in the ferrite region. *ISIJ Int.* **1997**, *37*, 807–814. [CrossRef]
24. Gupta, A.; Khatirkar, R.K.; Dandekar, T.; Jha, J.S.; Mishra, S. Recrystallization behavior of a cold rolled Ti–15V–3Sn–3Cr–3Al alloy. *J. Mater. Res.* **2019**, *34*, 3082–3092. [CrossRef]
25. Park, J.T.; Szpunar, J.A. Texture development during grain growth in non-oriented electrical steels. *ISIJ Int.* **2005**, *45*, 743–749. [CrossRef]
26. Huneus, H.; Günther, K.; Kochmann, T.; Plutniok, V.; Schoppa, A. Non-oriented magnetic steel with improved texture and permeability. *J. Mater. Eng. Perform.* **1993**, *2*, 199–203. [CrossRef]
27. Gheorghies, C.; Doniga, A. Evolution of texture in grain oriented silicon steels. *J. Iron Steel Res. Int.* **2009**, *16*, 78–83. [CrossRef]
28. Sidor, J.J.; Verbeken, K.; Gomes, E.; Schneider, J.; Calvillo, P.R.; Kestens, L.A.I. Through process texture evolution and magnetic properties of high Si non-oriented electrical steels. *Mater. Charact.* **2012**, *71*, 49–57. [CrossRef]
29. Jenkins, K.; Lindenmo, M. Precipitates in electrical steels. *J. Magn. Magn. Mater.* **2008**, *320*, 2423–2429. [CrossRef]
30. Salinas, J.J.; Salinas, A. Grain size and texture evolution during annealing of non-oriented electrical steel deformed in tension. *J. Mater. Eng. Perform.* **2015**, *24*, 2117–2125. [CrossRef]
31. De Campos, M.F.; Teixeira, J.C.; Landgraf, F.J.G. The optimum grain size for minimizing energy losses in iron. *J. Magn. Magn. Mater.* **2006**, *301*, 94–99. [CrossRef]

Disclaimer/Publisher's Note: The statements, opinions and data contained in all publications are solely those of the individual author(s) and contributor(s) and not of MDPI and/or the editor(s). MDPI and/or the editor(s) disclaim responsibility for any injury to people or property resulting from any ideas, methods, instructions or products referred to in the content.